Journal of Solid State Chemistry **148,** 333–341 (1999)
Article ID jssc.1999.8457, available online at http://www.idealibrary.com on IDEAL®

Structural Determination of the Charge Ordering Process in $Nd_{0.5}Ca_{0.5}Mn_{1-x}Cr_xO_3$ Manganites

W. Schuddinck,* G. Van Tendeloo,* A. Barnabe,† M. Hervieu,† and B. Raveau†

*EMAT, University of Antwerp (RUCA), Groenenborgerlaan, 171, B-2020 Antwerp, Belgium; and †Laboratoire CRISMAT, ISMRA, UMR 6508, Université de Caen, 6 Bd. du Maréchal Juin, 14050 Caen Cedex, France

Received January 20, 1999; in revised form July 1, 1999; accepted July 22, 1999

Structural properties of Cr-doped manganites $Nd_{0.5}Ca_{0.5}Mn_{1-x}Cr_xO_3$ with $0.02 \leq x \leq 0.07$ have been studied versus temperature by electron diffraction and high-resolution electron microscopy between 90 and 300 K. All compositions show an incommensurate superstructure over the whole temperature domain, despite the fact that they are ferromagnetic and conductive below 150 K. The q vector $(1/2 - \delta)a^*$ decreases with increasing temperature for all compositions x. For a given temperature q also decreases with x. Room-temperature high-resolution electron microscopy images show point defects similar to those observed for other $Ln_{0.5}Ca_{0.5}MnO_3$ manganites with $Ln = \{Pr, Nd, Sm\}$ and they also show intensity variations. Lattice images obtained at low temperature allow a better understanding of the charge ordering process. The low-temperature form of the Cr-doped manganites is not a perfectly doubled cell $\langle\langle 2a_p\sqrt{2} \times 2a_p \times a_p\sqrt{2}\rangle\rangle$, but defects inducing a tripled cell occur pseudo-periodically.

INTRODUCTION

In the past few years many studies have been carried out on the large series of manganites $Ln_{1-x}A_xMnO_3$ with $A = \{Ca, Sr, Ba, Pb\}$ which exhibit colossal magnetoresistance (CMR) properties (1–4). Compositions with $x = 0.5$ are of especially great interest because of the enormous complexity of the phenomenon of charge ordering (CO). It has been shown that this charge ordering has an influence on the magnetotransport properties of these materials (5–9). Earlier studies reported that the antiferromagnetic (AFM) to ferromagnetic (FM) transition, which is associated with the CO process, is accompanied in $La_{0.5}Ca_{0.5}MnO_3$ by a commensurate to incommensurate charge-ordering transition (10, 11) and recent studies prove that this is also the case for other elements of the *Ln* series (12, 13).

Among these manganites the $Nd_{0.5}Ca_{0.5}MnO_3$ composition is very interesting because it has been shown that for this material a phase transition takes place below T_{CO} (14, 15). When this composition is doped with Cr, the physical properties are altered (16). The Cr-doped materials become conducting at low temperatures ($T < 140$ K) and also the ferromagnetism becomes very strong. In the present paper, the influence of this chromium doping on the charge-ordering process is investigated by electron microscopy. Also the relationship between the physical measurements (resistivity and magnetization measurements) and the structural properties (electron diffraction (ED) study versus temperature) has been studied in the same way, as has been shown in recent papers (9, 12, 13).

EXPERIMENTAL PROCEDURE

The synthesis of polycrystalline $Nd_{0.5}Ca_{0.5}Mn_{1-x}Cr_xO_3$ samples ($x = 0$, 0.02, 0.05, 0.07, and 0.12) was carried out, starting from stoichiometric mixtures of Nd_2O_3, CaO, Cr_2O_3, and Mn_2O_3. The mixtures were heated at 1000°C to achieve decarbonation. Then, the samples were pressed into pellets and sintered, into two steps, at 1200 and 1500°C for 12 h. They were slowly cooled down to 800°C and finally quenched to room temperature.

The ED versus temperature study was carried out with a Philips CM20 electron microscope operating at 200 kV and equipped with a double-tilt liquid N_2 sample holder (tilt $\pm 30°$, $\pm 45°$, and 90 K $\leq T \leq$ 300 K). Dark-field lattice images were recorded at 95 K with a JEOL 2010 electron microscope fitted with a double-tilt cooling sample holder. The high-resolution electron microscopy study was performed with a JEOL 4000EX microscope operating at 400 kV. Fourier transform diffraction patterns were calculated using the program NIH Image.

In the electron diffraction study versus temperature all the patterns were recorded under the same experimental conditions, i.e., increasing the temperature from 90 to 300 K, in steps of 4 ($x = 0.02$) or 10 K, waiting for temperature stabilization during a minimum of 3 min before each ED recording, made with a constant electron beam adjustment. At higher temperatures longer exposure times were used to reveal the streaked and/or weaker spots. The

0022-4596/99 $30.00

positions of the reflections were measured in Adobe Photoshop after scanning of the negatives with an AGFA Arcus II scanner.

Resistance measurements were performed from room temperature down to 30 K by the four-probe method on sintered bars in the earth magnetic field. All bars have the same $2 \times 2 \times 10\ mm^3$ dimensions. The magnetization versus temperature was registered during heating with a vibrating sample magnetometer after a magnetic field of 1.4 or 0.01 T was applied at 4.2 K.

RESULTS AND DISCUSSION

Physical Properties

Our earlier study of the $Nd_{1-x}Ca_xMnO_3$ ($0.3 \leq x \leq 0.5$) series (15) has shown that for $x = 0.5$ a structural phase transition occurs from the orthorhombic room-temperature structure with *Pnma* symmetry to a low-temperature orthorhombic structure with *Pm*2*m* symmetry. This phase transition is accompanied by the appearance of sharp extra reflections at positions ($\frac{1}{2}$ 0 0) implying a doubling of the *a* parameter. A recent study of the $Ln_{0.5}Ca_{0.5}MnO_3$ manganites (12) showed that this is not an abrupt phase transition, but that between the two commensurate structures a large temperature region exists exhibiting a progressive transition with an incommensurate structure.

The magnetotransport properties of the oxides $Nd_{0.5}Ca_{0.5}Mn_{1-x}Cr_xO_3$ ($x = 0.00$, 0.02, 0.05, and 0.07) are summarized by the resistance measurements versus temperature ($R(T)$) curves and the magnetization ($M(T)$) curves displayed in Figs. 1 and 2, respectively. Two major differences between the doped and undoped compositions are noticed. First, the bending in the $R(T)$ curves, which is characteristic for CO (12, 17), disappears with increasing x and the Cr-doped materials are conducting for $T < 150$ K, whereas the undoped composition is insulating in this temperature region (Fig. 1). Conductivity means that there is mobility of the charges and this is not in agreement with a charge-ordering process, which assumes localization of the charges. Second, the M(T) curves show that the CE-type antiferromagnetism that is found in $Nd_{0.5}Ca_{0.5}MnO_3$ is progressively destroyed with increased Cr-doping and for the Cr-doped materials with $x > 0.02$ strong ferromagnetism at temperatures below 140 K appears (Fig. 2). Ferromagnetism suppresses charge ordering as can be seen by the "bump" at $T \approx 250$ K. This bump, which is characteristic for CO (12, 17), is clearly present for $x = 0.00$ and 0.02, is hardly seen for $x = 0.05$, and has completely disappeared for $x > 0.05$.

To obtain better insight into the behavior we have performed an electron microscopy study in a temperature range from 97 K to room temperature.

Charge Ordering in $Nd_{0.5}Ca_{0.5}Mn_{0.98}Cr_{0.02}O_3$

When $Nd_{0.5}Ca_{0.5}MnO_3$ is doped with small amounts of Cr, satellite reflections appear in the vicinity of the $\frac{1}{2}$ 0 0 superstructure reflections; i.e., the structure becomes incommensurate. The modulation vector can be written as $\mathbf{q} = (1/2 - \delta)\ \mathbf{a}^*$. The intensity of the incommensurate

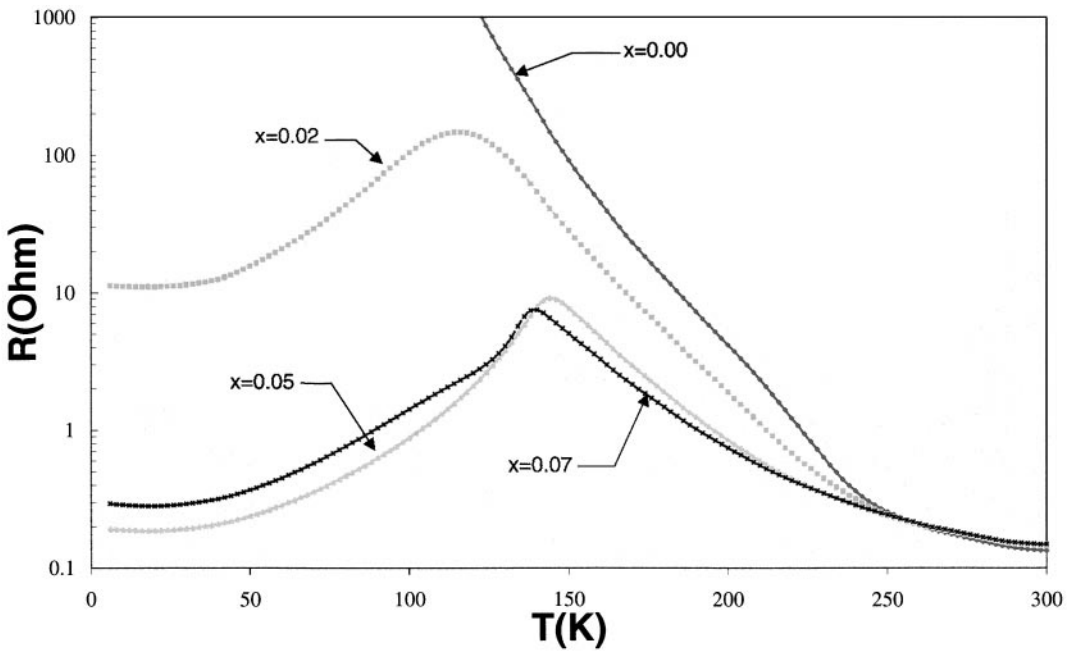

FIG. 1. Electric resistance in $Nd_{0.5}Ca_{0.5}Mn_{1-x}Cr_xO_3$ as a function of temperature.

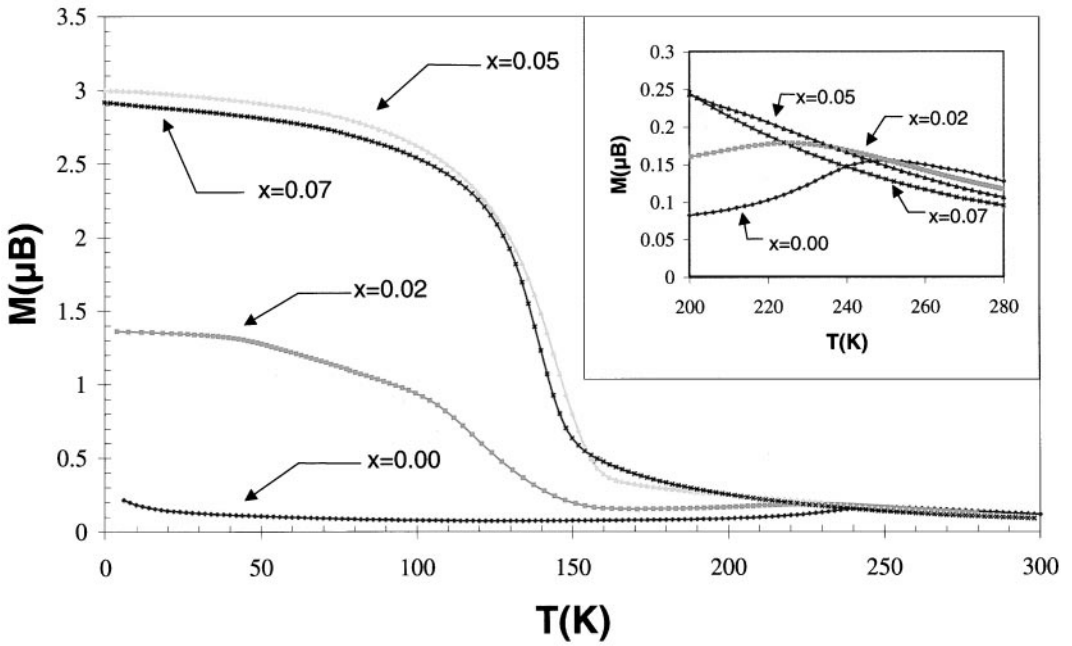

FIG. 2. Magnetization in $Nd_{0.5}Ca_{0.5}Mn_{1-x}Cr_xO_3$ as a function of temperature. Inset: Magnetization versus temperature near T_{CO}.

satellites scales with the intensity of the basic *Pnma* reflections as can be clearly seen from the enlarged Fig. 3. This shows that the satellites are not to be considered as a splitting of the $\frac{1}{2}$ 0 0 reflection, but as satellites of the basic *Pnma* spots. The $\frac{1}{2}$ 0 0 superstructure reflections present in the undoped material (15) then have to be considered as the end members of the series with $\mathbf{q} = 0.5\mathbf{a}^*$. Such modulation is best described using a notation based on four indices *hklm*: in Fig. 3 the $\bar{2}02\bar{1}$ satellite belongs to the $\bar{2}02$ reflection, whereas the 1011 satellite belongs to reflection 101. In some patterns also the second order satellites are visible, indicating that the modulation is not purely sinusoidal. Sometimes

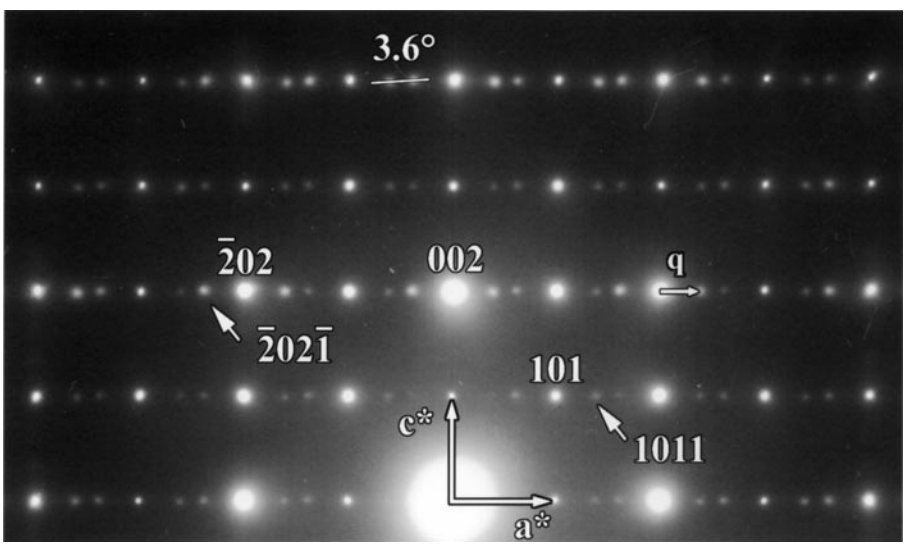

FIG. 3. [010] ED pattern of $Nd_{0.5}Ca_{0.5}Mn_{0.98}Cr_{0.02}O_3$ registered at a low temperature (97 K). The intense reflections are indexed in the $\langle\langle a_p\sqrt{2} \times 2a_p \times a_p\sqrt{2}\rangle\rangle$ cell. The weaker satellites of this *Pnma* reflection are indexed using a notation based on four indices *hklm*. These satellites sometimes have a component along **c*** as indicated by the 3.6° tilt angle.

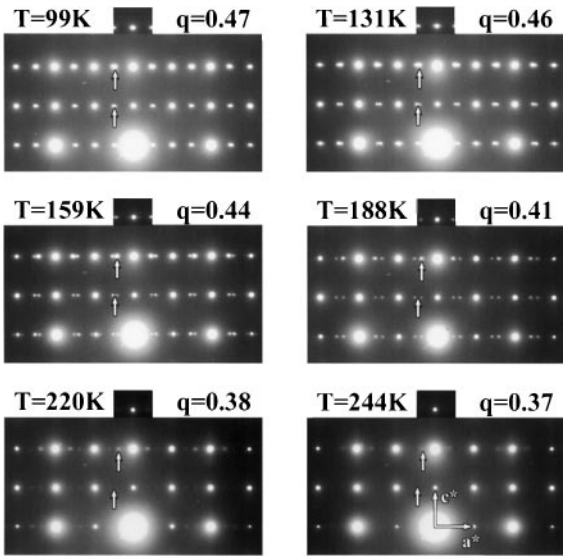

FIG. 4. Evolution with increasing temperature of the position of the $002\bar{1}$ reflection, indicated by the top white arrow with respect to the unsplit position (bottom white arrow) for the composition $Nd_{0.5}Ca_{0.5}Mn_{0.98}Cr_{0.02}O_3$.

the satellites are not exactly along **a***, but slightly inclined, i.e., **q** has a component along **c*** (indicated by the 3.6° tilt between two satellites in Fig. 3). The origin of this orientation anomaly will be discussed when considering the HREM at low temperature.

The position of the satellites changes continuously with temperature. This evolution is visible in the ED patterns of Fig. 4. The shift of the $002\bar{1}$ spot (upper arrow) is visualized with respect to the unsplit position (lower arrow). The evolution of the q value for $x = 0.02$ as a function of temperature is summarized in Fig. 5. This curve presents the "naked" measurements on a single sample during a heating run from 97 K to room temperature. The curve starts at $q = 0.472$ for $T = 97$ K and is then continuously descending until $q = 0.369$ is reached at $T = 244$ K. The presence of the apparent plateau at $q = 0.444$ near 160 K has to be considered with care; in fact, measurements on different samples did not reveal this plateau or showed a small plateau in a different temperature range. One of the reasons could be a problem of temperature stabilization, which is difficult to control, although the irradiating electron beam is kept constant during the several hours of the experiment. As the temperature increases the intensity of the satellites considerably decreases and at temperatures above $T = 244$ K, the incommensurate reflections become streaked along **a*** and the modulation vector can no longer be measured with enough precision. These streaked reflections, however, persist even at room temperature, but they are only visible in overexposed patterns. It should also be noted that different temperature runs on different crystals of the same nominal composition revealed a broad range of **q** vectors for a given temperature. For nominal $x = 0.02$ and $T = 97$ K, q values between 0.387 and 0.475 are measured. These differences in q values are certainly not completely due to the temperature

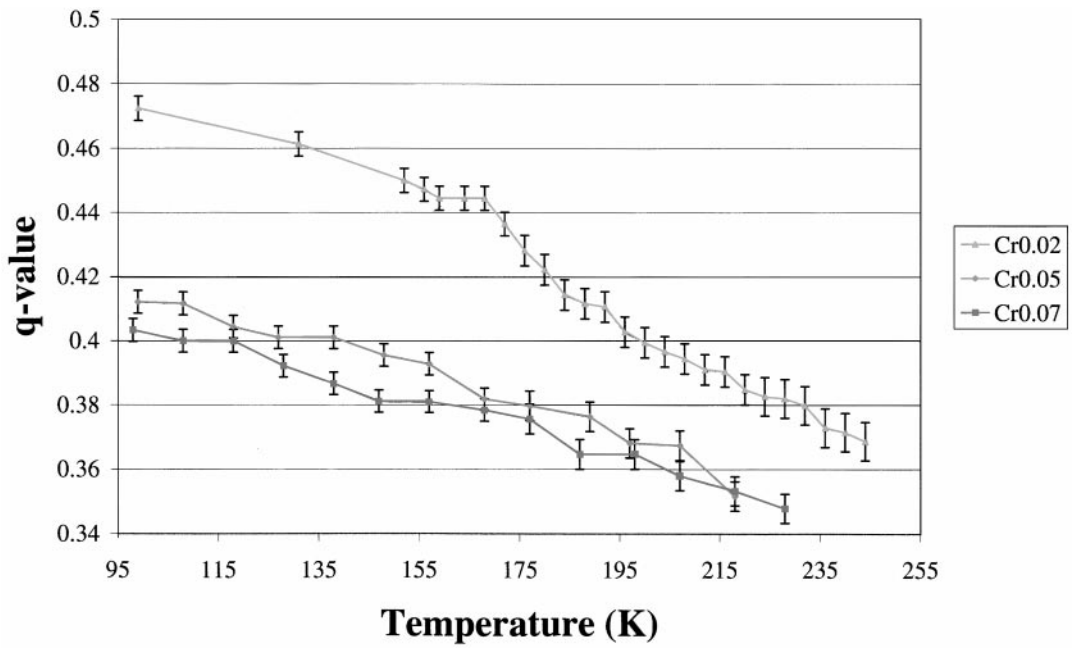

FIG. 5. The q value as a function of temperature for x values $x = 0.02$, 0.05, and 0.07. Above $T \approx T_{CO}$ the satellites become streaked along **a*** and the modulation vector can no longer be measured with enough precision.

difference between different crystals on the grid. Such differences are sometimes possible because the actual temperature is a combination of the temperature of the heating holder and the temperature induced by the electron beam. The latter strongly depends on the thermal contact of the sample with the carbon support. In Fig. 6, two temperature runs have been plotted for two crystals of the same batch, mounted on the same carbon grid. One notices a translation of the whole curve, so that the difference in q value is certainly not explained by a difference between measured and actual temperature. A straightforward explanation would be the presence of strong variations in the Cr-doping which may differ from grain to grain. Such large variations, however, would be surprising in view of the preparation method, the experience with related materials, and the EDX measurements. On the other hand it is also possible that there is no composition difference, but that one has a phase separation between different modulated phases (for a single composition). In this case, however, one would expect a preferential lock-in for commensurate q values, which is not the case here. Finally, one should note that within a single grain no domains with different **q** vectors were found; i.e., although q may vary between different grains, within a single grain q is constant.

This continuous descent of the q value could be correlated with the charge ordering process, as was also done for related compounds (9, 11–13). The fact that the intensity of the reflections drastically drops and becomes streaked at $T \approx 244$ K is in good agreement with the CO temperature indicated by the physical measurements at $T \approx 240$ K (inset Fig. 2).

It has to be noticed that the conductivity at temperatures below $T = 150$ K has no influence on the behavior of the modulation vector **q**. The descent of q is similar to that measured in the undoped compound (12), which is insulating. It should be noted, however, that the resistivity is measured on a large amount of material compared to the amount studied by electron microscopy and that only a slight fraction has to be conductive to give the measured result.

Lattice Images at 95 K for $Nd_{0.5}Ca_{0.5}Mn_{0.95}Cr_{0.05}O_3$

Low temperature ($T \cong 95$ K) high resolution electron microscopy (HREM) was performed for the compound with $x = 0.05$ in order to understand better the character of the charge-ordering process and the structure of the incommensurate phase. The [010] image shown in Fig. 8 shows a fringe system of (00l) planes, similar to that obtained for an over-oxidized $Sm_{0.5}Ca_{0.5}MnO_3$ (12). Two characteristic phenomena are clearly present:

- The sequence of bright and gray fringes is not regular. No well-ordered domains, where one bright fringe alternates with one gray fringe along **a** over a certain period, are visible. The distance between two bright fringes separated by one gray fringe is approximately 10.8 Å ($= 2 \times a_p\sqrt{2}$), in

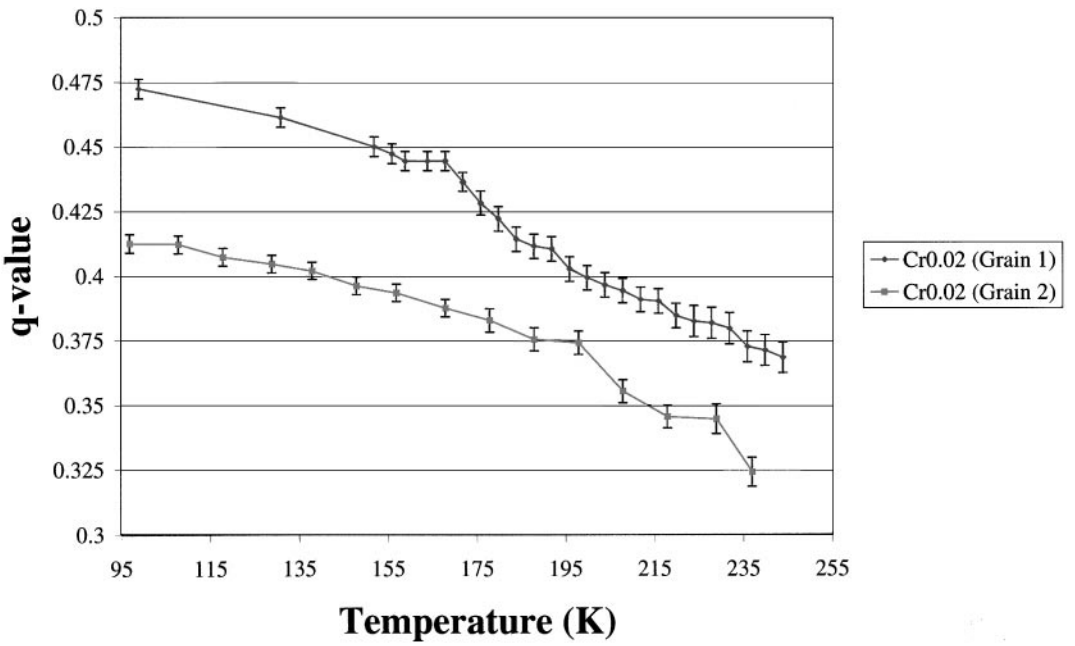

FIG. 6. The q value as a function of temperature for two different grains of the compound with nominal composition $x = 0.02$. This evolution indicates that the different q values measured in one compound are not completely due to a temperature difference between the different grains.

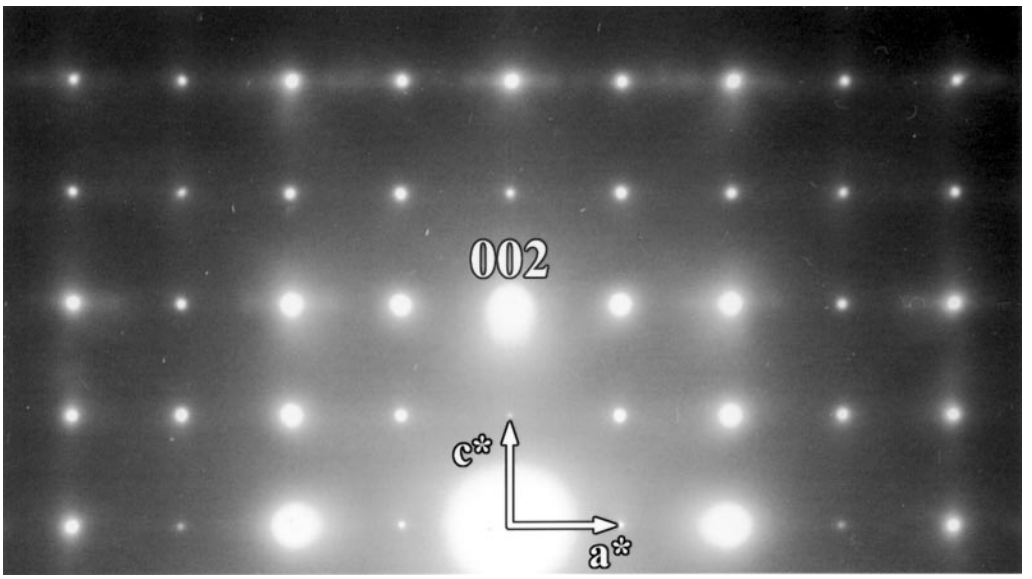

FIG. 7. [010] ED pattern of $Nd_{0.5}Ca_{0.5}Mn_{0.88}Cr_{0.12}O_3$ registered at 97 K showing the streaked satellites along **a***.

agreement with a doubling of the *a* parameter. But from time to time two adjacent gray or bright fringes appear with an interdistance of 5.4 Å ($= a_p\sqrt{2}$), as indicated on the figure by the two white arrows. We therefore have a uniform mixing of fringes separated by $2 \times a_p\sqrt{2}$ and fringes separated by $3 \times a_p\sqrt{2}$. This explains a **q** vector slightly smaller than 0.5.

- Occasionally a shift of the fringes along **a** occurs. This is illustrated by the black arrow in Fig. 8, where a gray fringe is connected to a bright fringe. The amplitude of the translation is $a_p\sqrt{2}$. As mentioned in (12) this shift implies that the modulation vector is no longer parallel to **a**, but has a small component along **c**. This explains the inclination of the satellites regarding **a*** observed in the ED patterns (see, e.g., Fig. 3).

The first phenomenon results from the fact that doping $Nd_{0.5}Ca_{0.5}MnO_3$ with small amounts of Cr causes a change in the ratio Mn^{3+}/Mn^{4+}. Toulemonde *et al.* (18) show that the formal charge of the doping element in this kind of composition is Cr^{3+}. It can be assumed that these Cr^{3+} substitute for the Mn^{3+}, so the composition can be written as $Nd_{0.5}Ca_{0.5}\{Cr^{3+}_{0.05}Mn^{3+}_{0.45}Mn^{4+}_{0.5}\}$ with $Mn^{4+}/Mn^{3+} > 1$. Other publications (9, 19) report that with such a ratio the possibility exists of having $q = 0.5 - \varepsilon$. On the other hand, the first commensurate structures with $q < 0.5$ are $q = 0.33$ and $q = 0.25$. Doping with Cr^{3+} destabilizes the commensurate structure $q = 0.5$ of $Nd_{0.5}Ca_{0.5}MnO_3$, but not enough to reach $q = 0.33$. Therefore an incommensurate structure is obtained.

The combination of these two phenomena strongly supports the structural model for the charge-ordering process proposed by Barnabé *et al.* (12), where such images are also interpreted by the presence of an excess Mn^{4+} ($Mn^4/Mn^{3+} > 1$). The additional Mn^{4+} species are ordered in the form of long-range ordered adjacenet $[Mn^{4+}O]_\infty$ layers and submitted to a shearing mechanism along **a**.

Evolution of the Charge-Ordering Process with Increased Cr-Doping

To verify whether charge ordering disappears when Cr-doping is increased — as expected from the $M(T)$ and $R(T)$ measurements — a systematic exploration of the modulated structure of the doped manganites $Nd_{0.5}Ca_{0.5}Mn_{1-x}Cr_xO_3$, following the same process as discribed above, has been carried out for four different x values from $x = 0.02$ to 0.12. The results for $x = 0.02$, 0.05, and 0.07 are summarized in Fig. 5, where the q values are drawn versus temperature ($97\ K \leq T \leq 270\ K$). Based on these results, the following remarks can be made:

(1) The structure is incommensurate for all x-values in spite of the fact that for $T < 140$ K the compounds become strongly ferromagnetic, which is a disadvantage for charge ordering. One would expect that when ferromagnetism became stronger charge ordering would be suppressed and the incommensurate reflections would become weaker; however, such a phenomenon is not observed in any of the crystals studied.

(2) In the $x = 0.05$ compound ferromagnetism and CO go together, but apparently this has no influence on the behavior of the q value, because a descent similar to that of the other x values is observed.

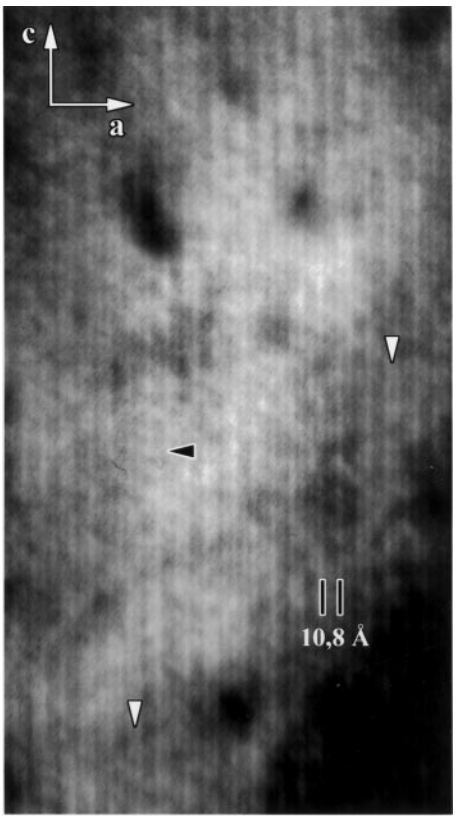

FIG. 8. Lattice image of a $Nd_{0.5}Ca_{0.5}Mn_{0.95}Cr_{0.05}O_3$ crystal recorded at 97 K. White arrows indicate the adjacent gray or bright fringes with an interdistance of 5.4 Å. The black arrow indicates a shift of a bright fringe along **a***.

(3) For each nominal composition, a variation of the modulation vector is observed in different crystals, but within a single crystal the modulation vector is constant.

(4) The q value is always incommensurate and decreases as the chromium doping (x) is increased. This strongly suggests that the undoped phase has also to be considered as a modulated structure, but with a commensurate **q** vector ($q = 0.5$), as mentioned in (13, 20). It also shows that increased doping of $Nd_{0.5}Ca_{0.5}MnO_3$ with Cr "kills" the CO. As x is increased Cr^{3+} elements substitute for Mn^{3+}, so the lattice of the Mn is increasingly perturbed and ordering of Mn^{3+} and Mn^{4+} becomes more difficult. Finally, when x is high enough CO completely disappears as can be seen for $x = 0.12$, where no clear modulation reflections are observed, even at $T = 97$ K; only a weak streaking along **a*** with a maximum around $q \approx 0.35$ is present (Fig. 7).

(5) The temperature where the reflections broaden and become streaked along **a*** is in good agreement with the T_{CO} obtained by the physical properties for all x values.

Room Temperature High-Resolution Imaging

The compounds were also studied at room temperature by HREM. Figure 9a is a [010] HREM image of the $x = 0.02$ compound showing an area that consists of a square-like array of bright dots, 2.7 Å spaced along **a** and **c**, which is usually observed for perovskite-related compounds. The grains are well crystallized without extended defects. "Point-like" defects in the form of abnormally dark dots appear. Very often, these defects are clustered, but no clear periodicity can be determined. Such defects have also been reported in manganites like $Ln_{0.7}A_{0.3}MnO_3$, $Ln_{0.75}A_{0.25}MnO_3$ with $Ln = Pr$, $A = Ca$ or Sr (20), $Nd_{1-x}Ca_xMnO_3$ with $0.3 \leq x \leq 0.5$ (15), and $Sm_{0.5}Ca_{0.5}Mn_{1-x}Cr_xO_3$ with $0.00 \leq x \leq 0.07$ (13). Our observations show that this type of defect is an intrinsic feature of this family of materials. In Fig. 9a also intensity variations are randomly observed along **a** and **c** (lines indicated by white arrows). These sequences of extra white dots, however, are not at the origin of the observed diffuse streaking along **a*** in the corresponding electron diffraction pattern, a "left-over" of the charge ordering. Since the intensity variations occur randomly, they also produce no noticeable effect on the corresponding Fourier transform (Fig. 9c). The origin of the intensity modulations is most probably related to the presence of point-like defects, lining up along the **a** and **c** directions.

CONCLUSION

This study of the oxides $Nd_{0.5}Ca_{0.5}Mn_{1-x}Cr_xO_3$ shows that the charge-ordering process is progressive and corresponds to a broad temperature range where the structure is incommensurate. The incommensurable **q** vector decreases continously as temperature is increased and no lock-in at commensurate values is observed. With increasing temperature also the intensity of the incommensurate satellites reduces and at T_{CO} the satellite reflections become streaked along **a***. This temperature is in good agreement with the T_{CO} obtained by physical properties measurements. With increased Cr-doping the **q** vector decreases, but within one compound **q** values vary over a broad range. The fact that these Cr-doped compounds are ferromagnetic and conductive at low temperature seems to have no influence on the behavior of the modulation vector **q**. Lattice images obtained at low temperature allow us to better understand the characteristics and features of the charge-ordering process, but further investigations with better direct spatial resolution at lower temperatures and diffraction measurements below 100 K are necessary to obtain a complete image of this complex mechanism and its relationship to phenomena like conductivity and ferromagnetism.

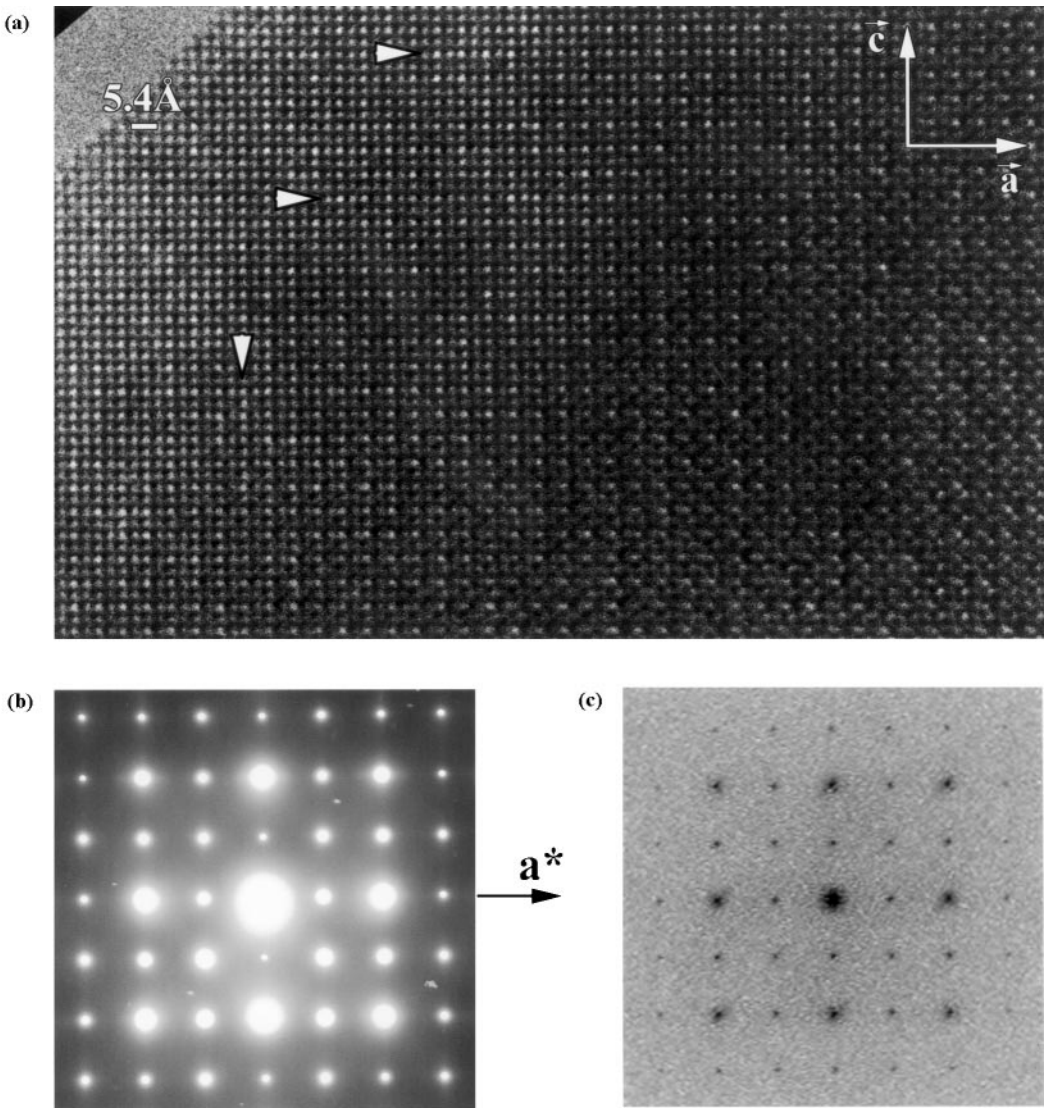

FIG. 9. (a) [010] HREM image of $Nd_{0.5}Ca_{0.5}Mn_{0.98}Cr_{0.02}O_3$ at room temperature. 'Point-like' defects appear in the form of abnormally dark dots. Intensity variations, which are randomly observed along **a** and **c**, are indicated by white arrows. (b) Experimental ED pattern of the same area as (a) showing a diffuse streaking along **a***, a 'leftover' of the charge ordering. (c) ED obtained by FFT of (a). No diffuse streaking along **a*** is observed here.

ACKNOWLEDGMENTS

W. Schuddinck is grateful to the FWO for financial support. This research has been performed within the framework of IUAP 4/10.

REFERENCES

1. R. M. Kusters, J. Singleton, D. A. Keen, *et al*., *Physica B* **155,** 362 (1989).
2. S. Jin, T. H. Tiefel, M. McCormack, *et al*., *Science* **264,** 413 (1994).
3. P. Schiffer, A. P. Ramirez, W. Bao, *et al*., *Phys. Rev. Lett*. **75,** 3336 (1995).
4. R. von Helmont, J. Wecker, B. Holzapfel, *et al*., *Phys. Rev. B* **71,** 2231 (1993).
5. Y. Tokura, H. Kuwahara, Y. Moritomo, *et al*., *Phys. Rev. Lett*. **76,** 3184 (1996).
6. Y. Tomioka, A. Asamitsu, Y. Moritomo, *et al*., *Phys. Rev. Lett*. **74,** 5108 (1995).
7. Z. Jirak, S. Krupicka, Z. Simsa, *et al*., *J. Magn. Magn. Mater*. **53,** 153 (1985).
8. V. Caignaert, F. Millange, M. Hervieu, *et al*., *Solid State Commun*. **99,** 173 (1996).
9. Y. Murakami, D. Shindo, H. Chiba, *et al*., *J. Solid State Chem*. **140,** 331 (1998).
10. P. G. Radaelli, D. E. Cox, M. Marezio, *et al*., *Phys. Rev. B* **55,** 3015 (1997).
11. C. H. Chen and S.-W. Chenong, *Phys. Rev. Lett*. **76,** 4042 (1996).
12. A. Barnabé, M. Hervieu, C. Martin, *et al*., *J. Appl. Phys.* **84,** 5506 (1998).

13. A. Barnabé, M. Hervieu, C. Martin, *et al*., *J. Mater. Chem.* **8,** 1405 (1998).
14. H. Taguchi, M. Nagao, and M. Shinada, *J. Solid State Chem.* **76,** 284 (1998).
15. O. Richard, W. Schuddinck, G. Van Tendeloo, *et al*., *Acta Crystallogr. Sect. A* **55,** 704 (1999).
16. A. Barnabé, A. Maignan, M. Hervieu, *et al*., *Appl. Phys. Lett*. **71,** 3907 (1997).
17. M. Hervieu, A. Barnabé, C. Martin, *et al*., *Eur. Phys. J. B* **8,** 31 (1999).
18. O. Toulemonde, F. Studer, A. Barnabé, *et al*., *Eur. Phys. J. B* **4,** 159 (1998).
19. Y. Murakami, D. Shindo, H. Chiba, *et al*., *Phys. Rev. B* **55,** 1 (1997).
20. M. Hervieu, G. Van Tendeloo, V. Caignaert, *et al*., *Phys. Rev. B* **53,** 14274 (1996).